Available online at www.sciencedirect.com
ScienceDirect
Journal of Sound and Vibration 324 (2009) 520–538
JOURNAL OF SOUND AND VIBRATION
www.elsevier.com/locate/jsvi

Modelling and multi-criteria optimisation of passive seat suspension vibro-isolating properties

I. Maciejewski[a,*], L. Meyer[b], T. Krzyzynski[a]

[a]*Koszalin University of Technology, Department of Mechatronics and Applied Mechanics, Raclawicka 15-17, Koszalin 75-256, Poland*
[b]*Isringhausen GMBH and CO. KG, Testlaboratory, An der Bega 58, Lemgo, 32657 DE, Germany*

Received 18 January 2008; received in revised form 18 February 2009; accepted 18 February 2009
Handling Editor: C.L. Morfey
Available online 25 March 2009

Abstract

In this paper mathematical models of a conventional and modified passive suspension of working machine seats are presented. A seat with a viscous-elastic passive suspension, whose vibro-isolation properties are improved by a modification of an air-spring and shock absorber, is the object of modelling and simulation. For a vibration isolating system defined in such a way, a set of poly-optimal solutions was determined using two opposing criteria: the acceleration of the vehicle operator and the relative displacement of seat suspension. The power spectral density of the acceleration of the seat with respect to sample excitations on the working machine floor are presented. Transmissibility functions for a passive conventional suspension and the corresponding modified seat are also presented. The modified seat showed improved performance over the conventional seat in the 0–4 Hz frequency range.

1. Introduction

Truck drivers and operators of earth-moving machines during their work are exposed to vibration, most often coming from road surface unevenness. The vibration experienced in a typical earth-moving machine cab usually occurs at frequencies from 0 to 20 Hz [1]. Such a phenomenon is very undesirable, because the human body has a number of natural frequencies in this range. The consequences for operators are: loss of concentration, tiredness and decrease of the effectiveness of the work being performed. Vibration discomfort for heavy-duty machine operators coincides with eigenfrequencies of the human body. The most dangerous frequency range of external vertical vibration for the seated human body is between 4 and 9 Hz, because there are several body eigenfrequencies in that range [2–6]. Most passive suspensions in conventional seats amplify these low frequency vibrations [7].

In the case of a typical working machine without axle suspension, a seat suspension is the only system which can protect the operator from vibration. A passive seat suspension amplifies vibration at frequencies close to its natural resonance frequencies. The first natural frequency of typical, passive seats with an air-spring and

*Corresponding author. Tel.: +48 943 478 395.
E-mail addresses: igor.maciejewski@tu.koszalin.pl (I. Maciejewski), lutz.meyer@isri.de (L. Meyer), tkrzyz@tu.koszalin.pl (T. Krzyzynski).

0022-460X/$ - see front matter © 2009 Elsevier Ltd. All rights reserved.
doi:10.1016/j.jsv.2009.02.021

Nomenclature

A_{add}	surface of additional air reservoir, m^2
A_{as}	surface of air-spring, m^2
A_{ef}	effective area of air-spring, m^2
b	critical pressure ratio
c_1, c_2	weight coefficients of an optimal control function
C	critical conductance, $m^3/(s\,Pa)$
d_1	linear damping coefficient, $N\,s/m$
d_2	quadratic damping coefficient, $N\,(s/m)^2$
d_3	cubic damping coefficient, $N\,(s/m)^3$
d_d	lower limit of suspension travel without contact with bottom buffers, m
d_u	upper limit of suspension travel without contact with top buffers, m
E	expected value
EM3	excitation signal representative for wheel loaders
EM6	excitation signal representative for crawler loaders or crawler dozers
F_{as}	air-spring force, N
F_b	overall end stop buffers force, N
F_{bd}	bottom end stop buffers force, N
F_{bu}	top end stop buffers force, N
F_d	shock-absorber force, N
F_{ff}	friction force, N
F_g	gravity force, N
$F_{\text{objective}}$	objective function
g	gravity constant, m/s^2
h_0	initial height of air-spring, m
J	objective function of optimal control
k_{d1}	linear stiffness coefficient (bottom buffers), N/m
k_{d3}	cubic stiffness coefficient (bottom buffers), N/m^3
k_{ff}	stiffness of a seat suspension at the change of movement direction, N/m
k_{u1}	linear stiffness coefficient (top buffers), N/m
k_{u3}	cubic stiffness coefficient (top buffers), N/m^3
m	suspended mass, kg
m_{as0}	initial air mass inside an air-spring, kg
m_{add0}	initial air mass inside an additional air reservoir, kg
m_s	mass of suspension system affixed to suspended mass, kg
$\dot{m}$	mass flow rate, kg/s
p_{as}	air pressure inside an air-spring, Pa
p_{add}	air pressure inside an additional air reservoir, Pa
p_0	atmospheric pressure, Pa
R	gas constant, $J/(kg\,K)$
SEAT	seat effective amplitude transmissibility factor
T	temperature of flowing air, K
T_{add}	air temperature inside an additional air reservoir, K
T_{as}	air temperature inside an air-spring, K
T_{norm}	temperature of standard conditions, K
T_w	wall temperature of an air-spring and additional air reservoir, K
u_1, u_2	linear scaling functions
w	weighting coefficient
WNP	excitation signal similar to the white, band limited noise
V_{add}	volume of additional air reservoir, m^3
V_{as}	air-spring volume, m^3
x	displacement of suspended mass, m
x_s	displacement of excitation, m
$(x-x_s)_{\max}$	maximum relative displacement of suspension system (peak to peak value), m
$\ddot{x}_{\text{RMS}}$	effective acceleration of suspended mass (root mean square value), m/s^2
α_{add}	overall heat transfer coefficient of an additional air reservoir, $W/(m^2\,K)$
α_{as}	overall heat transfer coefficient of an air-spring, $W/(m^2\,K)$
β	first parameter regulating the shape of a hysteresis model, m^{-1}
γ	second parameter regulating the shape of a hysteresis model, m^{-1}
δ_{as}	reduction ratio of an air-spring
δ_d	reduction ratio of a shock-absorber
κ	adiabatic coefficient
ρ_{norm}	density of standard conditions, kg/m^3

hydraulic shock-absorber is between 1 and 2 Hz. Such a poor efficiency of passive seats for low frequencies and high amplitudes of excitation signal is a hazard to a driver's health and in effect shortens his working life.

Due to the poor effectiveness of passive seats at the system resonance frequencies, further investigations into improved seat performance are required. Such investigations are being performed in seat suspension research centres and they result in new ideas and solutions [7–18].

The application of pneumatic, nonlinear elements allows for improved vibro-isolating properties of the suspension. This kind of system is characterized by relatively simple regulation of stiffness and damping of the pneumatic suspension by adjusting air pressure. The adjustable pressure inside the air-spring can cause constant static deflection of a suspension system at different loads. Whereas the regulation of air pressure changes the stiffness of the suspension system, so its eigenfrequency can be moved. The features mentioned above are desired especially for automotive vibro-isolating systems where low and constant eigenfrequency with changeable loads is required.

Toyofuku et al. [18] analysed the dynamic characteristics of the air-spring with an additional air reservoir for an electronically controlled vehicle air suspension system. The application of an additional air reservoir makes the stiffness characteristics of theair-spring softer and in consequence decreases the natural frequency of the system. A correctly designed vibro-isolating system should have a low eigenfrequency, but some stiffness has to be sustained. The air-spring has minimal damping, therefore this kind of element applied to suspension systems requires an external shock-absorber. A damping force can be generated by airflow throttling between the additional air reservoir and the air-spring.

Hostens et al. [9] presented an improved design of air suspension for seats in mobile agricultural machines. The improved system uses an air-spring, an additional air reservoir volume to lower the system natural frequency and air damping with a throttle valve. The authors concentrated on the reduction of harmful vibrations transmitted to a driver, but did not take into account the opposing requirement of minimising the suspension deflection.

The optimal design of nonlinear, pneumatic suspension systems by shaping of the visco-elastic characteristics is not published yet. However, the separate influence of effects such as damping force, additional air reservoir and throttling between the air-spring and additional air reservoir are known, often based on linear models, and published in Refs. [9,18–20]. The simultaneous influence of a shock-absorber force with a change of an air-spring force by the additional air reservoir and throttling of the air-flow, especially for nonlinear models, has not been reported in the literature.

The objective of this paper was to present an effective way of modelling and optimising the vibro-isolating properties of a passive seat suspension.

2. Opposite criteria of vibro-properties of the seat

The main problem of seat suspension control strategy is the existence of two opposite requirements:

- minimization of absolute acceleration of a loaded seat (Fig. 1a) and
- minimization of relative displacement of a seat suspension (Fig. 1b).

On one hand, the absolute acceleration on the seat should approach zero, in order to protect the driver's health. On the other hand, the maximum relative displacement between the seat and floor of operator's cabin should approach zero as well, in order to ensure the controllability of the working machines. The best compromise between opposite criteria creates a complex, nonlinear optimisation problem.

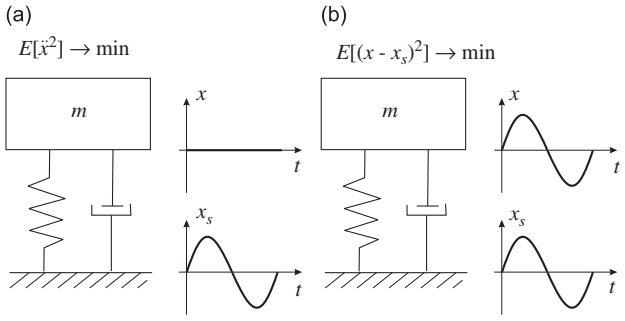

Fig. 1. Opposite requirements for vibro-isolating properties of seat suspension: (a) minimization of the absolute acceleration of a loaded seat and (b) minimization of the relative displacement of the seat suspension.

An appropriate control policy for the seat suspension is by minimizing the objective function [21]:

$$J = c_1 E[\ddot{x}^2] + c_2 E[(x - x_s)^2] \rightarrow \text{minimum} \tag{1}$$

where c_1 and c_2 are weighting coefficients which depend on the significance of opposite criteria, $E[\ddot{x}^2]$ is the expected value of the squared seat acceleration and $E[(x - x_s)^2]$ is the expected value of the squared relative displacement between the seat x and the cabin floor x_s, respectively (Fig. 1).

3. Modelling of the passive seat suspension with an air-spring and hydraulic shock-absorber

3.1. Conventional passive seat suspension

For the purpose of this paper, a typical suspension system was chosen (Fig. 2). This system consists of a shear guidance mechanism, an air-spring, a hydraulic shock-absorber and end-stop buffers. The damped resonance effect is produced by the spring force combined with the shock-absorber force. Amplification of vibration in the 0–2 Hz frequency range was observed. At higher frequencies the desired behaviour of the seat suspension was reached and vibrations transmitted by the seat were reduced significantly.

3.2. Physical model

In Fig. 2 a physical model of a conventional passive seat suspension system containing an air-spring and a hydraulic shock-absorber is shown. The seat suspension model takes into account the spring force F_{as}, the damping force F_d, the forces from end-stop buffers F_b limiting the maximum relative displacement, the overall friction force of suspension system F_{ff} and the gravity force of suspending mass F_g. In the simplified physical model, the inertia of shear mechanism of the suspension system was neglected.

3.3. Mathematical model

The equation of motion for a passive seat suspension system, as an equilibrium of forces acting on the suspended mass, reads

$$(m + m_s)\ddot{x} = F_{as} + F_d + F_{ff} + F_b + F_g \tag{2}$$

The force coming from the air-spring and acting in the vertical direction with the reduction ratio δ_{as}, is described as the product of an effective area of the air-spring A_{ef} and the relative air pressure $p_{as} - p_0$ [7,13]:

$$F_{as} = \frac{1}{\delta_{as}} A_{\text{ef}}(p_{as} - p_0) \tag{3}$$

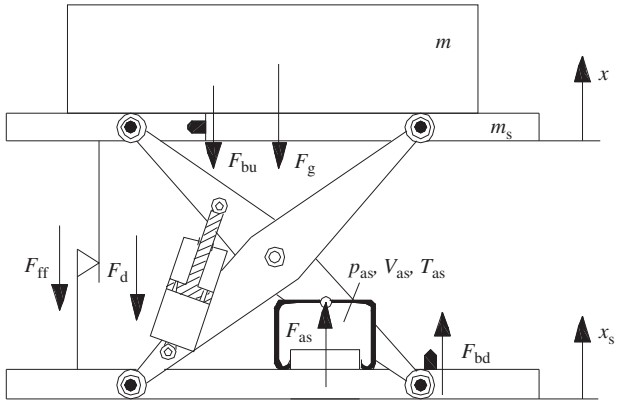

Fig. 2. Physical model of the conventional passive seat suspension.

The actual value of the air pressure in the air-spring, at a variable volume V_{as} and temperature T_{as}, is defined as the first-order differential equation [22–24] and can be written in the following form:

$$\dot{p}_{as}V_{as} + \kappa p_{as}\dot{V}_{as} + (\kappa - 1)A_{as}\alpha_{as}(T_{as} - T_w) = 0 \tag{4}$$

In addition to the pressure change component, the heat transfer through the boundaries of the pneumatic capacity is also taken into account. Other effects on the heat transfer, such as convection or radiation are neglected. Here, the adiabatic coefficient κ is assumed equal to 1.4, the wall temperature T_w is estimated as equal to the ambient temperature, A_{as} is the wall surface of the air-spring, whereas the heat transfer coefficient α_{as} across the air-spring wall is calculated [23]. The simplified model of the air-spring volume is described as the cylinder configuration, at the initial height h_0:

$$V_{as} = A_{\text{ef}}\left(\frac{x - x_s}{\delta_{as}} + h_0\right) \tag{5}$$

The air temperature T_{as} in the air-spring is calculated on the basis of ideal gas law [22,23]. The actual pressure p_{as} in the air-spring and its actual volume V_{as} define the temperature of constant gas mass m_{as0}:

$$T_{as} = \frac{p_{as}V_{as}}{m_{as0}R} \tag{6}$$

The equation describing the viscous damping force, acting in the vertical direction on a suspended mass, is written as polynomial approximation of measurement results in the relative velocity domain $x - x_s$ [8] and divided by a reduction ratio δ_d:

$$F_d = -\frac{1}{\delta_d}\left(d_3\left(\frac{\dot{x} - \dot{x}_s}{\delta_d}\right)^3 + d_2\left(\frac{\dot{x} - \dot{x}_s}{\delta_d}\right)^2 + d_1\left(\frac{\dot{x} - \dot{x}_s}{\delta_d}\right)\right) \tag{7}$$

where d_i are polynomial coefficients.

According to the Bouc–Wen model, the friction force F_{ff} describes the hysteretic properties of the suspension system [8]:

$$\dot{F}_{ff} = -k_{ff}(\dot{x} - \dot{x}_s) + \gamma|\dot{x} - \dot{x}_s|F_{ff} + \beta(\dot{x} - \dot{x}_s)|F_{ff}| \tag{8}$$

where k_{ff} is positive stiffness influences the magnitude of the hysteresis, γ and β give the hysteresis shape and describe viso-elastic properties of the seat suspension system when the movement direction is changed.

The forces of end-stop buffers, i.e. the bottom F_{bd} and the top F_{bu}, are modelled as a cubic, nonlinear stiffnesses (k_{d3}, k_{d1} and k_{u3}, k_{u1}, respectively) acting in a specified range of the seat suspension relative displacement: the bottom buffer $d_d > x - x_s$, the top buffer $d_u < x - x_s$ [8]:

$$F_{bd} = k_{d3}(x - x_s - d_d)^3 + k_{d1}(x - x_s - d_d), \quad d_d > x - x_s \tag{9}$$

$$F_{bu} = k_{u3}(x - x_s - d_d)^3 + k_{u1}(x - x_s - d_u), \quad d_u < x - x_s \tag{10}$$

The stiffness coefficients: k_{d3}, k_{d1}, k_{u3}, k_{u1} can be determined with the help of a static force–deflection test of the suspension system. Finally, the overall force coming from the end-stop buffers F_b, limiting the maximum relative displacement of suspension system is given by

$$F_b = F_{bd} + F_{bu} \tag{11}$$

The gravity force F_g is proportional to the sum of the value of suspended mass m and the mass of suspension system affixed to suspended mass m_s:

$$F_g = -(m + m_s)g \tag{12}$$

3.4. Evaluation of the model parameters

The evaluation of numerical values of the mathematical model parameters was based on measurements. The effective area of the air-spring was evaluated by calculating the measured air-spring force per the measured

static air pressure inside the air-spring (Eq. (3)). The force sensor was affixed to the upper part of the air-spring which has reciprocated with triangle cycling at a frequency of 1 mHz and an amplitude of ±30 mm. The air pressure in a variable volume of the air-spring was measured by the pressure sensor. The experimental set-up used and the measurement results are shown in Fig. 3.

The temperature of air inside the air-spring was defined by simplified calculation (Eq. (6)); however, its thermal characteristics depends on the heat transfer through the wall of the air-spring (Eq. (4)). The calculation of overall heat transfer coefficient α_{as} between the air in the air-spring and the air in the atmosphere separated by rubber material of the air-spring defines this effect.

The measured dimensions of the shear guidance mechanism allowed the calculation of the motion of the air-spring and the motion of the shock-absorber in relation to the motion of the suspension system. The reduction ratios δ_{as} (Eq. (3)) and δ_d (Eq. (5)) were evaluated as a proportion of the motions of the suspension system relative to the air-spring and the suspension system relative to the shock-absorber. The change of these reduction ratios is technically realized by the different geometry of the air-spring and the shock-absorber between the arms of the shear guidance mechanism. The reduction ratios of the air-spring and the shock-absorber define the forces acting on the suspended mass, which are reduced by the shear guidance mechanism.

The force of shock-absorber in velocity domain was evaluated by sinusoidal cycling of the damper. The shock-absorber was moved vertically at a frequency of 1.67 Hz and an amplitude of ±12.5 mm. The force and velocity sensors were used for measuring the actual damping force at different velocities of the shock-absorber. The experimental set-up and the measured force in the relative velocity domain are shown in Fig. 4. The least-squares approximation of the measured data enabled calculation of the polynomial coefficients d_1, d_2, d_3 of Eq. (7).

The coefficients of the friction force model (Eq. (8)) were determined with the help of the force–deflection measurement with triangular cycling of the suspension system. The force sensor was affixed to the upper part of the suspension system (Fig. 5a). The lower part of the suspension system was excited at a frequency of 1 Hz and an amplitude of ±2 mm. The displacement sensor was installed for evaluating the actual suspension deflection. The measured hysteresis of the friction force in displacement domain (Fig. 5b) was fitted to the simulation results by appropriate selection of the model parameters k_{ff}, γ, β.

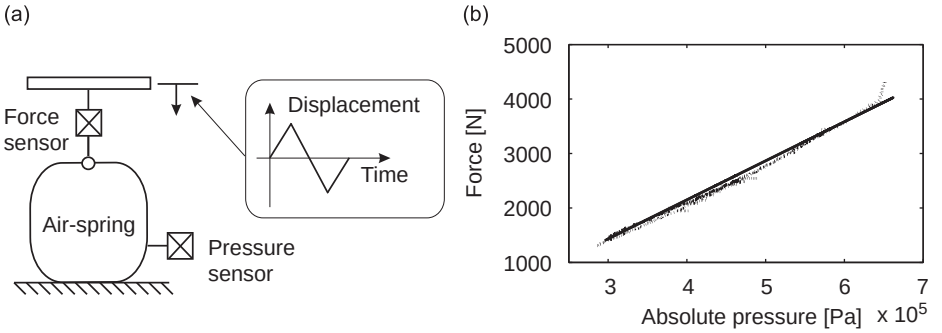

Fig. 3. Experimental set-up for the evaluation of the air-spring force (a), corresponding results (b): simulation model (——), measurement (.....).

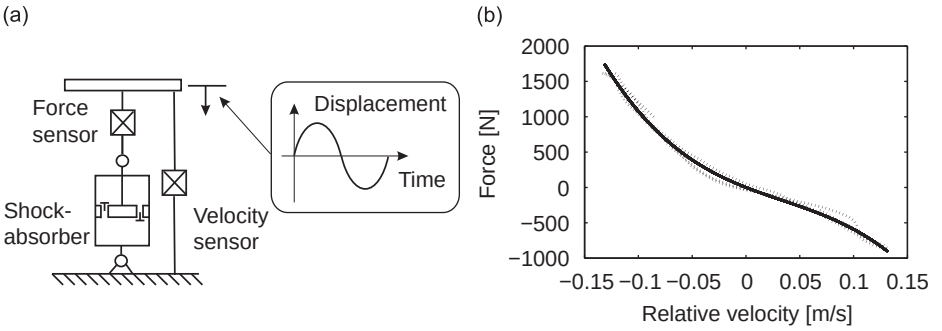

Fig. 4. Experimental set-up for the evaluation of the shock-absorber force (a), corresponding results (b): simulation model (——), measurement (.....).

The force–deflection measurement of the suspension system with the end stop buffers installed was performed to determine the stiffness characteristics of the buffers (Fig. 6). The air-spring was initially pumped and the air-spring volume was closed. The suspension system was deflected with triangle cycling at a frequency of 2 mHz and an amplitude of ±80 mm. The force and displacement of the suspension system were measured during this test. The overall force of the bottom end stop buffers was approximated by Eq. (9) and the overall force of the top end stop buffers was approximated by Eq. (10) whose stiffness coefficients k_{d3}, k_{d1}, k_{u3}, k_{u1} are estimated by the least-squares method.

Each parameter value used by the seat suspension model is shown in Appendix A. Moreover, all calculations presented in the paper are related to a specific type of seat, which means that all parameters have to be evaluated experimentally for a specific seat type.

3.5. Model verification

The experimental set-up consisted of a hydraulic shaker and a vibration platform with the seat suspension system. During the evaluation of seat suspension behaviour, the following excitation signals were used:

- WNP—a signal similar to the white, band limited noise in the range of frequency 1–12.5 Hz,
- EM3—a signal at low frequencies and high amplitudes of vibration, representative for wheel loaders [1] and
- EM6—a signal at high frequencies and low amplitudes of vibration, representative for crawler loaders or crawler dozers [1].

During the tests, the following signals were measured: the acceleration of vibration platform, the acceleration of the load mass, the relative displacement of the suspension system and the absolute displacement of vibration platform. Based on these signals, the power spectral densities of the acceleration and transmissibility functions were evaluated and are shown in Fig. 7.

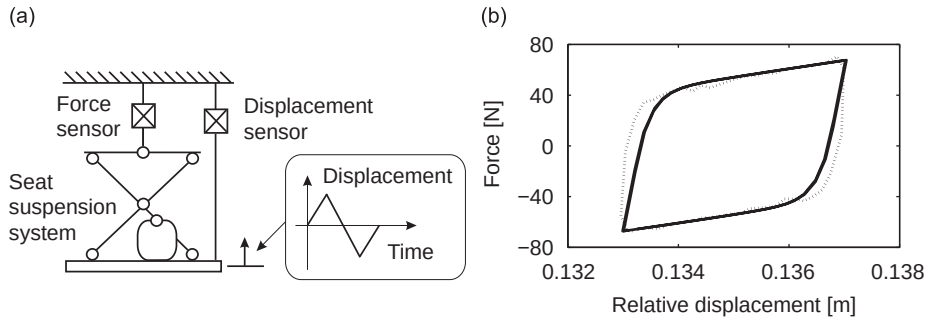

Fig. 5. Experimental set-up for the evaluation of the suspension friction (a), corresponding results (b): simulation model (——), measurement (.....).

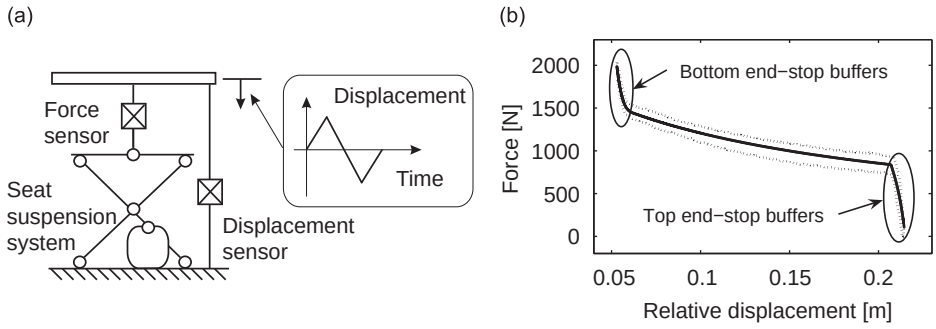

Fig. 6. Experimental set-up for the evaluation of the buffers force (a), corresponding results (b): simulation model (——), measurement (.....).

The results of numerical simulations conducted on the conventional seat suspension were very close to the results measured experimentally. The worst agreement between vibration amplitudes can be observed at the resonance frequency of the passive seat suspension. The particular SEAT factors [1,3], maximum relative displacements and relative errors are presented in Table 1.

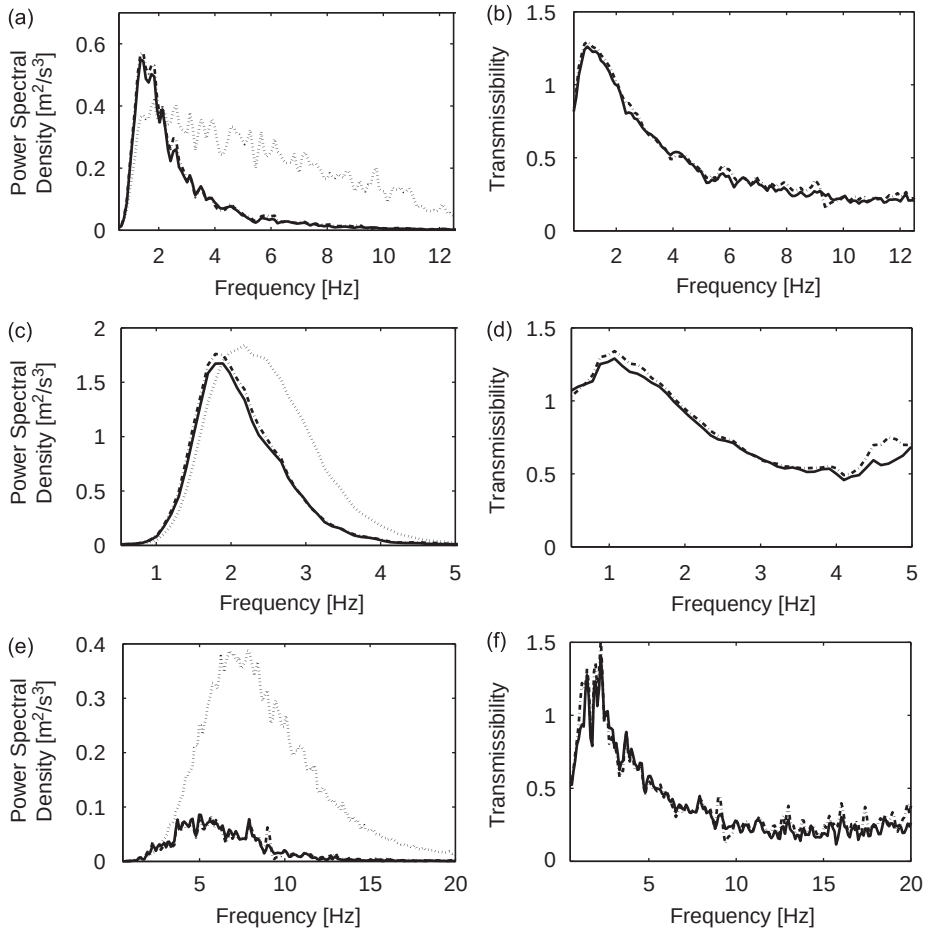

Fig. 7. Measured (- - -) and simulated (——) power spectral densities for excitation signals: (a) WNP, (c) EM3, (e) EM6 and transmissibility curves of seat suspension for excitation signals (·····): (b) WNP, (d) EM3, (f) EM6.

Table 1
Simulated and measured SEAT factors, maximum relative displacements and relative errors for the conventional seat suspension for excitation signals: WNP, EM3, EM6.

	Simulation		Measurement		Relative error	
	SEAT factor	Maximum relative displacement (mm)	SEAT factor	Maximum relative displacement (mm)	SEAT factor (%)	Maximum relative displacement (%)
WNP	0.484	71	0.500	68	3	4
EM3	0.766	84	0.789	83	3	1
EM6	0.389	10	0.388	11	0	9

4. Possibilities for improving the vibro-isolation properties of seat suspension

4.1. Modified seat suspension

Different possibilities for improving seat dynamical behaviour were then considered in the light of an example suspension system, with assumed constructional properties described earlier, by assessing the geometrical and physical nonlinearities. In a modified seat suspension system the following changes were applied: an additional air reservoir was placed in an air-spring by the throttle and a change in the characteristic of the shock-absorber was made. Preliminary simulations and measurements indicated significant improvements in vibro-isolation properties for a passive seat.

4.2. Physical model of the modified passive seat suspension

A model of a seat suspension modified by means of an additional, non-deformable air reservoir, and also by means of a change of the shock-absorber force F_d in a relative velocity domain was developed (Fig. 8). The throttling of the air-flow mass $\dot{m}$ between the additional air volume V_{add} and the air-spring volume V_{as} introduced an additional damping force to the system.

4.3. Mathematical model of the modified passive seat suspension

Equations of motion of the modified passive seat suspension took a form similar to the case of the conventional passive seat model (Eq. (2)). The actual value of air pressure p_{as} in the air-spring, connected with additional air reservoir was obtained from the following equation [22–24]:

$$\dot{p}_{as}V_{as} + \kappa p_{as}\dot{V}_{as} + (\kappa - 1)A_{as}\alpha_{as}(T_{as} - T_w) = \kappa R\dot{m}T \tag{13}$$

where κ is the adiabatic coefficient, R is the gas constant and $\dot{m}$ is the mass of air-flow at temperature T, between the additional air volume V_{add} and air-spring volume V_{as}. The air temperature T_{as} in the air-spring was calculated from actual pressure p_{as}, variable air-spring volume V_{as} and initial mass of air m_{as0}, using the ideal gas law [22,23]:

$$T_{as} = \frac{p_{as}V_{as}}{(m_{as0} + \int \dot{m}\,\mathrm{d}t)R} \tag{14}$$

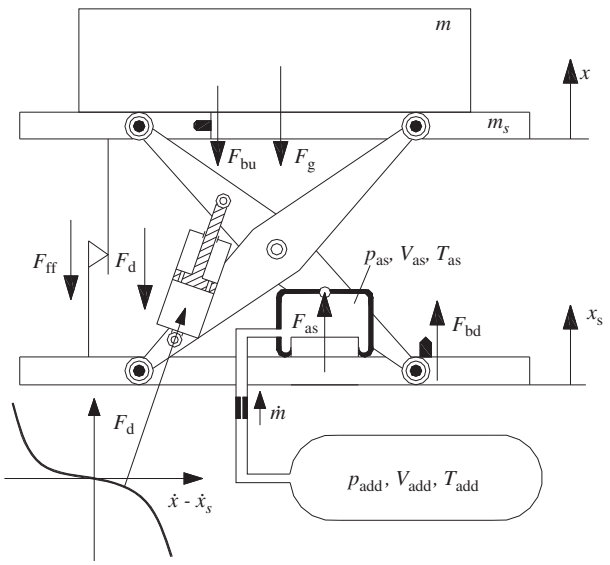

Fig. 8. Physical model of the modified passive seat suspension.

The actual value of the air pressure p_{add} in a constant additional air reservoir, connected with the air-spring was calculated from the following equation [22–24]:

$$\dot{p}_{\mathrm{add}} V_{\mathrm{add}} + (\kappa - 1) A_{\mathrm{add}} \alpha_{\mathrm{add}} (T_{\mathrm{add}} - T_w) = -\kappa R \dot{m} T \tag{15}$$

where $\dot{m}$ is the mass of air-flow, at temperature T, between the air-spring volume V_{as} and additional air volume V_{add}. The air temperature T_{add} in the additional air reservoir was defined for the actual pressure p_{add}, the constant volume V_{add} and the initial mass of air m_{add0}, using the ideal gas law [22,23]:

$$T_{\mathrm{add}} = \frac{p_{\mathrm{add}} V_{\mathrm{add}}}{(m_{\mathrm{add0}} + \int \dot{m}\,\mathrm{d}t) R} \tag{16}$$

In Eqs. (13) and (15) the term $\dot{m}T$ represents pneumatic resistance, the description of which contains the critical conductance C and critical pressure ratio b as its parameters [25]. With the aid of parameters C and b, and provided that $p_{as} > p_{\mathrm{add}}$, the mass flow at temperature T, from air-spring to additional air reservoir, was calculated as follows (subcritical range $p_{\mathrm{add}}/p_{as} > b$):

$$\dot{m}T = C p_{as} \rho_{\mathrm{norm}} \sqrt{\frac{T_{\mathrm{norm}}}{T_{as}}} \sqrt{1 - \frac{\left(\frac{p_{\mathrm{add}}}{p_{as}} - b\right)^2}{(1-b)^2}} T_{as} \tag{17}$$

and in the supercritical range $p_{\mathrm{add}}/p_{as} \leqslant b$:

$$\dot{m}T = C p_{as} \rho_{\mathrm{norm}} \sqrt{\frac{T_{\mathrm{norm}}}{T_{as}}} T_{as} \tag{18}$$

When $p_{as} < p_{\mathrm{add}}$, the mass flow at temperature T, from additional air reservoir to air-spring, was calculated as follows (subcritical range $p_{as}/p_{\mathrm{add}} > b$):

$$\dot{m}T = C p_{\mathrm{add}} \rho_{\mathrm{norm}} \sqrt{\frac{T_{\mathrm{norm}}}{T_{\mathrm{add}}}} \sqrt{1 - \frac{\left(\frac{p_{as}}{p_{\mathrm{add}}} - b\right)^2}{(1-b)^2}} T_{\mathrm{add}} \tag{19}$$

and in the supercritical range $p_{as}/p_{\mathrm{add}} \leqslant b$:

$$\dot{m}T = C p_{\mathrm{add}} \rho_{\mathrm{norm}} \sqrt{\frac{T_{\mathrm{norm}}}{T_{\mathrm{add}}}} T_{\mathrm{add}} \tag{20}$$

where ρ_{norm} and T_{norm} are the ISO standard values [25].

Other models of forces acting in the suspension system; i.e. the shock-absorber force F_d, the friction force F_{ff}, the end-stop buffers force F_b and the gravity force F_g were determined in the same way as in the case of the conventional passive seat model.

4.4. Parameters variation

In order to check the influence of the following effects: the additional air reservoir, the throttling of the air-flow between additional air reservoir and air-spring and the shock-absorber force, the ranges of parameters were taken as

- additional air volume $V_{\mathrm{add}} = 0.3-1.5\,\mathrm{l}$,
- throttling critical conductance $C = 0.46-1.47\,\mathrm{l/(sbar)}$ and
- reduction ratio of shock-absorber force $\delta_d = 2.5-3.86$.

The additional air reservoir decreases the stiffness coefficient, and in consequence the eigenfrequency of seat suspension is shifted to the lower values [7]. With the use of the additional air reservoir, the suspension system becomes softer and the relative displacement increases. The additional damping force coming from throttling

of the air-flow and the harder shock-absorber characteristics were helpful in restricting the amplification of vibration amplitude in resonance. In Fig. 9 the graphical illustration of the parameter variation and its influence on seat suspension behaviour is shown.

The forces of an air-spring connected with additional air reservoir were obtained for uniform motion of the suspension system at low velocity 0.16 mm/s (Fig. 9a). The increase of non-deformable air volume V_{add} resulted in a lowering of the variation of pressure inside the air-spring, so the variation of its force decreased. The forces of the shock-absorber were obtained from sinusoidal motion of the suspension at a frequency of 3.2 Hz and an amplitude of ±25 mm (Fig. 9b). The increase in the reduction ratio of the shock-absorber force δ_d resulted in the lowering of the nonlinear damping force in the suspension system. The characteristics of the air-flow between the air-spring and the additional air reservoir were obtained for a constant pressure in the air-spring of 8 bar and by increasing the pressure in the additional air reservoir at 0.48 bar/min (Fig. 9c). The increase of critical conductance C of the throttle resulted in the higher mass flow rate, so the additional air-damping introduced into the suspension system decreased.

4.5. Simulation results

Based on many numerical simulations with the use of white noise as the excitation signal, the effective acceleration (RMS) of the isolated mass and the maximum relative displacement of the suspension system were evaluated. In Fig. 10 results obtained for different parameters of the seat suspension model; i.e. the value of additional air volume V_{add}, the value of critical conductance C and for different reduction ratios of shock-absorber force δ_d, are shown.

As shown by the results obtained by means of numerical simulations, decreasing of acceleration of suspended mass goes together with significant increases in the maximum relative displacement, cf. Fig. 10. The simulation results show that the effective acceleration of isolated mass decreases when the maximum relative

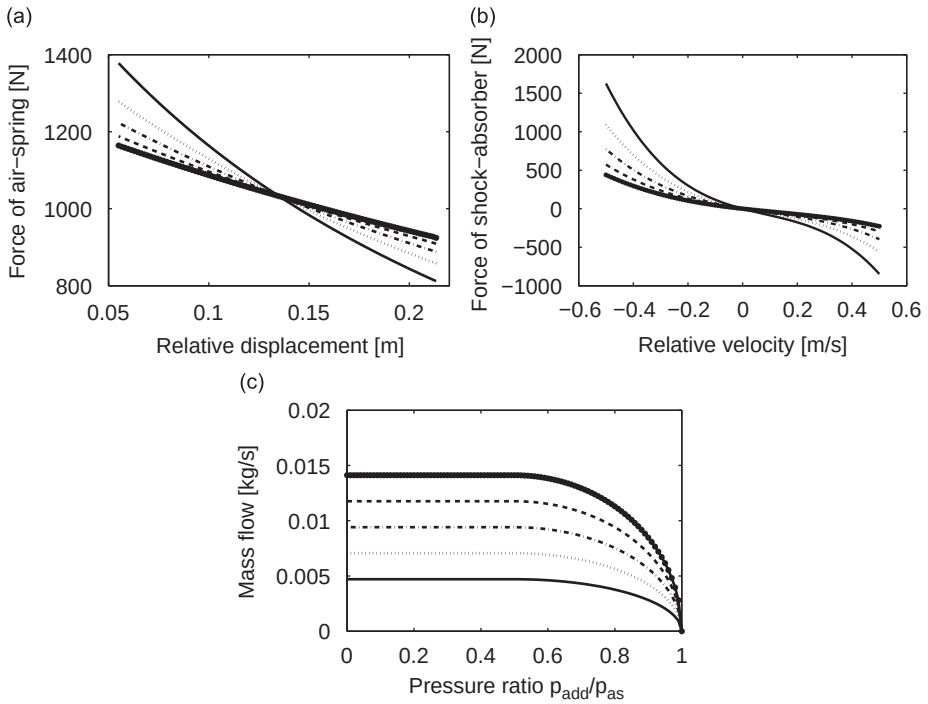

Fig. 9. Parameter variation in the assumed ranges: (a) force of air spring for different additional air volumes $V_{add} = 0.31$ (——), $V_{add} = 0.61$ (·····), $V_{add} = 0.91$ (-·-·-), $V_{add} = 1.21$ (----), $V_{add} = 1.51$ (●), (b) force of shock-absorber for different reduction ratios $\delta_d = 2.50$ (——), $\delta_d = 2.84$ (·····), $\delta_d = 3.18$ (-·-·-), $\delta_d = 3.52$ (----), $\delta_d = 3.86$ (●), (c) mass flow for different throttling critical conductances $C = 0.461$/(sbar) (——), $C = 0.681$/(sbar) (·····), $C = 0.911$/(sbar) (-·-·-), $C = 1.141$/(sbar) (----), $C = 1.371$/(sbar) (●).

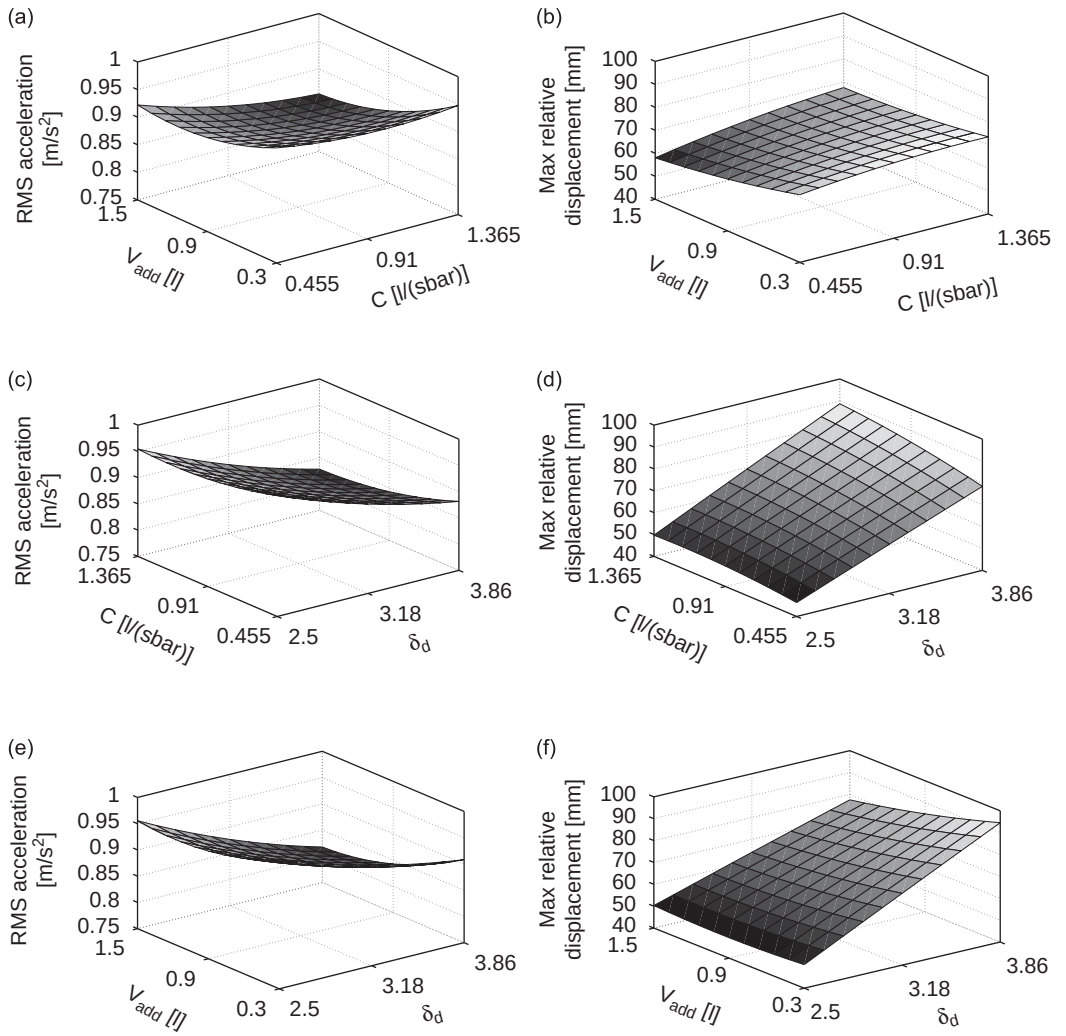

Fig. 10. Effective value of the isolated mass acceleration at different parameters of simulation model: (a) throttling critical conductance—additional air volume, (c) reduction ratio of shock-absorber force—throttling critical conductance, (e) reduction ratio of shock-absorber force—additional air volume and the maximum relative displacement of suspension system at different parameters of simulation model: (b) throttling critical conductance—additional air volume, (d) reduction ratio of shock-absorber force—throttling critical conductance, (f) reduction ratio of shock-absorber force—additional air volume.

displacement of suspension system increases. As a consequence of the above the issue of correct parameter evaluation arises: additional air volume, throttling critical conductance and reduction ratio of shock-absorber force.

5. Multi-criteria optimisation of seat suspension properties

The daily whole-body vibration exposure limit value of RMS acceleration standardised to an 8-h reference period is defined in current European Law as $1.15\,m/s^2$ [3]. The maximum value of suspension system travel including contact with the end stop buffers is typically about 120 mm based on experience of the machine operators. For higher suspension travel there is the risk that the operator might lose control of the machine. If the range of suspension travel exceeds the value of about ± 50 mm, than a hit in the end stop buffers occurs. Striking the end-stops creates shocks, so the forces transmitted by the suspension system to the machine operator increase. As a consequence of this effect, the RMS acceleration measured on the seat also increases.

There is not a comfort criteria standardised for selection of the trade-off between the RMS acceleration and the maximum relative displacement of suspension system. However the most ''comfortable'' trade-off can be selected with the help of multi-criteria optimisation.

5.1. Problem formulation

In order to optimize the seat suspension vibro-isolating properties, the optimisation procedure with the scalar objective function was defined as [24]

$$F_{\text{objective}} = wu_1(\ddot{x}_{\text{RMS}}) + (1-w)u_2((x-x_s)_{\max}) \rightarrow \text{maximum} \tag{21}$$

where w is the weight coefficient describing an influence of the particular vibro-isolating criteria (the acceleration of the vehicle operator and the relative displacement of seat suspension) on the global value of the objective function. The optimisation criteria were defined as follows: effective acceleration $\ddot{x}_{\text{RMS}}$ and maximum relative displacement $(x-x_s)_{\max}$:

$$\ddot{x}_{\text{RMS}} = f(V_{\text{add}}, C, \delta_d) \rightarrow \text{minimum} \tag{22}$$

$$(x-x_s)_{\max} = f(V_{\text{add}}, C, \delta_d) \rightarrow \text{minimum} \tag{23}$$

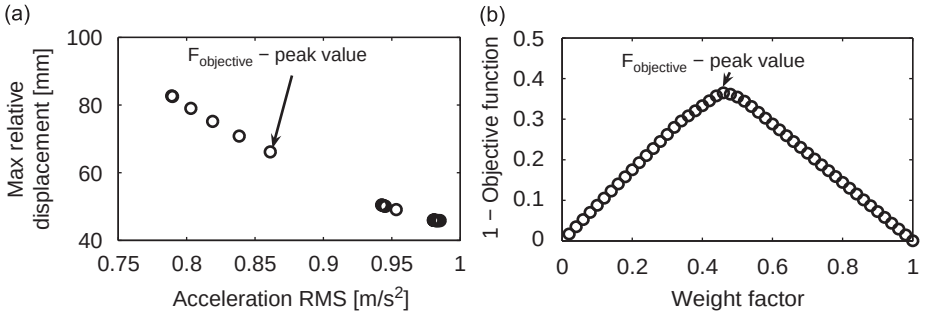

Fig. 11. (a) Poly-optimal points distribution for opposite vibro-isolating criteria at different weight coefficient and (b) values of corresponding objective function.

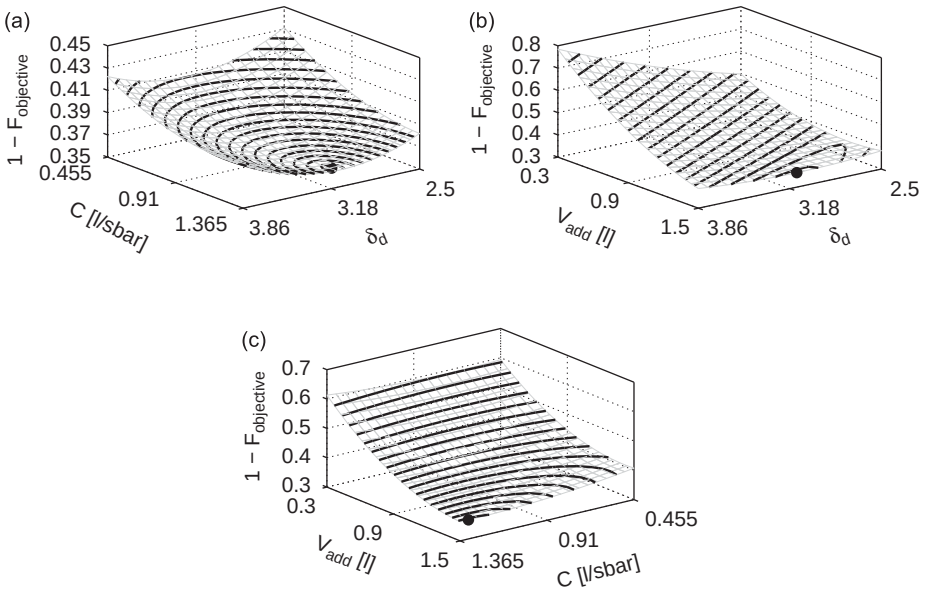

Fig. 12. Three-dimensional contour plot (——) of the objective function for a weight factor 0.46 and at the constant decision variables: (a) $V_{\text{add}} = 1.5$l, (b) $C = 1.321$/(sbar), (c) $\delta_d = 3.13$; optimum of the objective function for a weight factor 0.46 (•).

The equations describing particular criteria were obtained as polynomial functions determined from numerical simulations in the following domains: the value of additional air volume V_{add}, the value of throttling critical conductance C and the reduction ratio of shock-absorber force δ_d. In order to normalize the range of the opposing criteria (Eqs. (22) and (23)), the linear scaling functions were used [24]:

$$u_1(\ddot{x}_{\text{RMS}}) = \frac{(\ddot{x}_{\text{RMS}})_{\max} - \ddot{x}_{\text{RMS}}}{(\ddot{x}_{\text{RMS}})_{\max} - (\ddot{x}_{\text{RMS}})_{\min}} \tag{24}$$

$$u_2((x - x_s)_{\max}) = \frac{((x - x_s)_{\max})_{\max} - (x - x_s)_{\max}}{((x - x_s)_{\max})_{\max} - ((x - x_s)_{\max})_{\min}} \tag{25}$$

The constraints of the optimisation procedure were the ranges of decision variables: V_{add}, C and δ_d only. In Fig. 11a the multi-criteria optimisation is presented as the opposing criteria values for different weight coefficients. The corresponding objective function is shown in Fig. 11b.

The control of the vibro-isolation properties of the seat suspension was enabled by changing the values of the decision variables: V_{add}, C and δ_d. The maximum compromise between minimising the acceleration acting on the driver $\ddot{x}_{\text{RMS}}$ and reducing the maximum relative displacement $(x - x_s)_{\max}$ was obtained for a weight factor 0.46. For lower values of the weight factor, the limiting of acceleration is obtained, but for higher weight factor values the relative displacement is reduced significantly, cf. Fig. 11.

The shape of the objective function (Eq. (21)) was analysed in order to prove that its optimum in the decision variable domain was a global one. In the assumed ranges of the decision variables the shape was

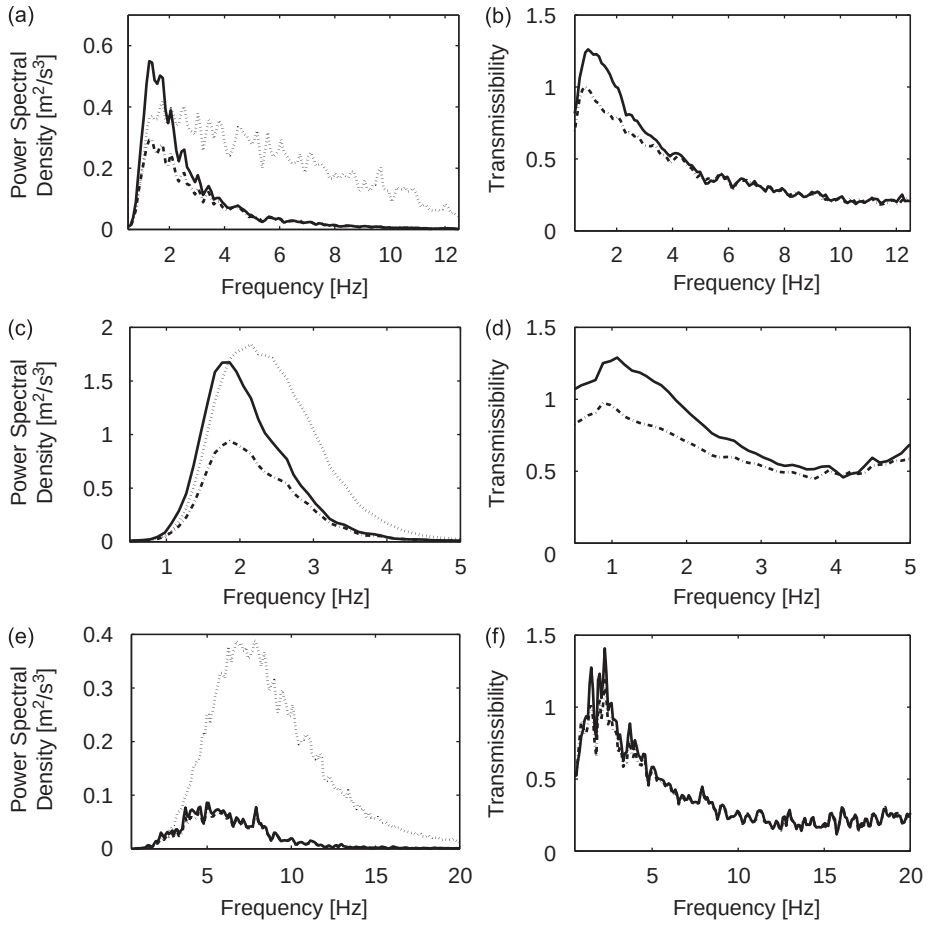

Fig. 13. Simulated power spectral densities of conventional (——) and modified (-·-·-) seat suspensions for excitation signals (·····): (a) WNP, (c) EM3, (e) EM6 and transmissibility curves of seat suspensions for excitation signals: (b) WNP, (d) EM3, (f) EM6.

convex. Three-dimensional contour plots of the objective function are shown in Fig. 12. The optimum of the objective function at a weight coefficient 0.46 was found for the decision variables: $V_{\text{add}} = 1.5\text{l}$, $C = 1.32\text{l}/(\text{sbar})$, $\delta_d = 3.13$. Moreover, the optimisation procedure began from different starting points within the decision variables range. The sought optimum of the objective function has occurred only once.

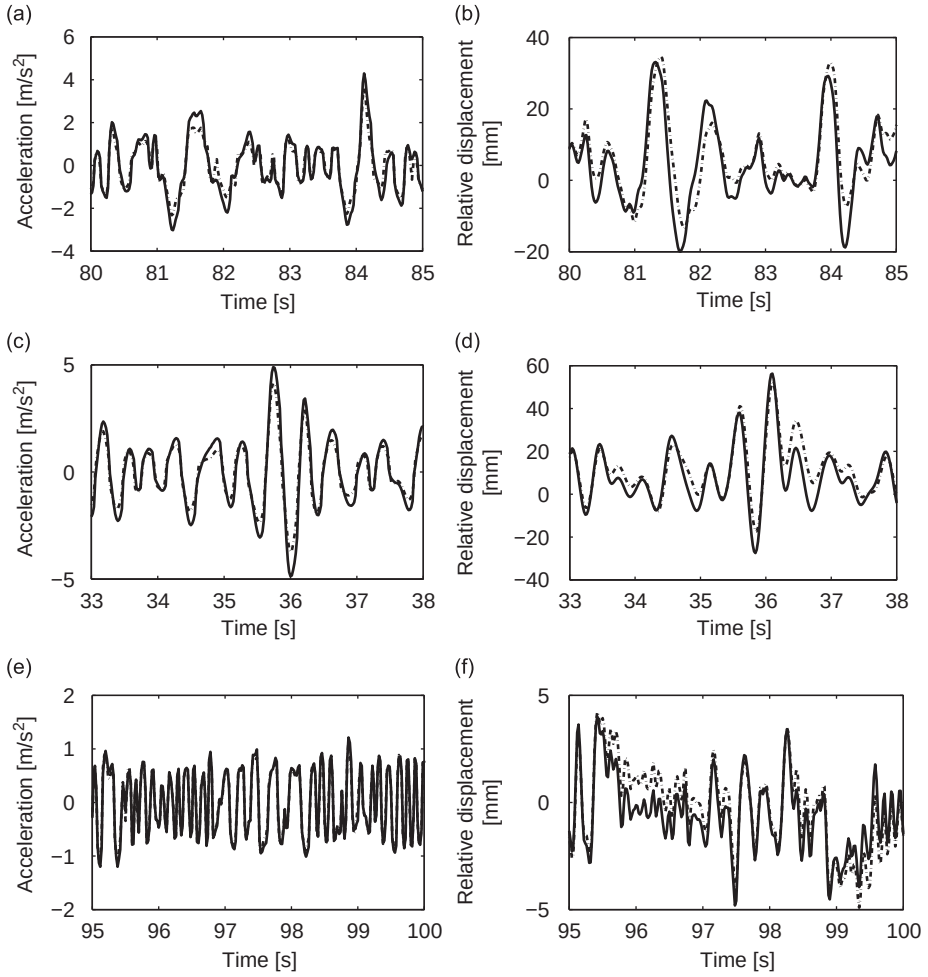

Fig. 14. Simulated accelerations of conventional (——) and modified (– – –) seat suspension for excitation signals (·····): (a) WNP, (c) EM3, (e) EM6 and relative displacements of seat suspension for excitation signals: (b) WNP, (d) EM3, (f) EM6.

Table 2
Simulated SEAT factors, maximum relative displacements and improvements of the modified seat suspension in comparison with the conventional one for excitation signals: WNP, EM3, EM6.

	Conventional		Modified		Improvement	
	SEAT factor	Maximum relative displacement (mm)	SEAT factor	Maximum relative displacement (mm)	SEAT factor (%)	Maximum relative displacement (%)
WNP	0.484	71	0.431	67	11	6
EM3	0.766	84	0.622	78	9	7
EM6	0.389	10	0.374	10	4	0

5.2. Simulation results

In Fig. 13 the simulation results obtained for the decision variables with the weight coefficient equal to 0.46 (maximum of objective function) are presented. The simulation results showing the accelerations and the maximum relative displacements of the suspension system as a function of time are presented in Fig. 14.

The results of the simulated, modified seat suspension demonstrated that the SEAT factor and the opposite maximum relative displacement are lower for excitation signals WNP and EM3. For the EM6 excitation signal (higher frequency range) the improvement was insignificant. The best performance of the modified seat suspension system was observed at the resonance frequency of the corresponding conventional seat. In Table 2 the selected SEAT factors [1], maximum relative displacements and improvements are presented.

5.3. Measurement results

The dynamic behaviour of the modified seat suspension was investigated using the experimental test set-up described in Section 3.4. Moreover, the effect of the machine operator mass on the system performance was taken into account. The measurement results of the modified and optimized seat suspension at different loads: $m = 50$ and 120 kg are shown in Figs. 15 and 16, respectively.

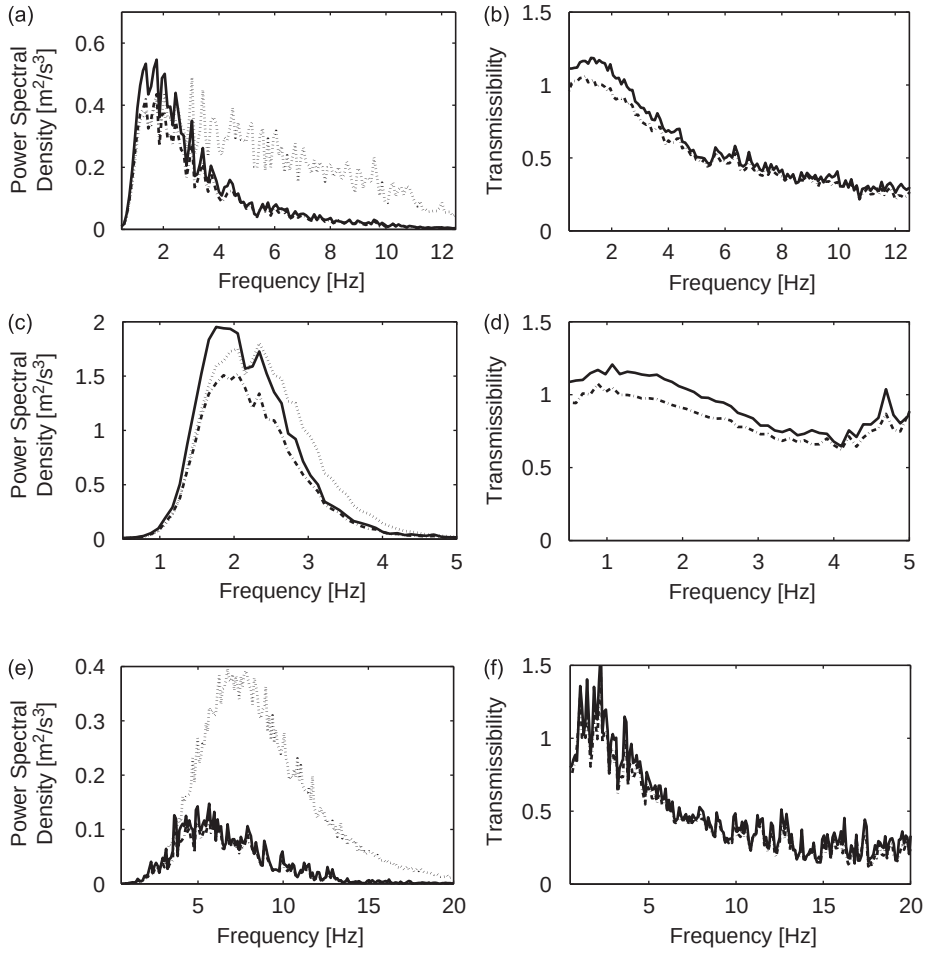

Fig. 15. Measured power spectral densities of conventional (——) and modified (- - -) seat suspensions for excitation (·····) signals: (a) WNP, (c) EM3, (e) EM6 and transmissibility curves of seat suspensions for excitation signals: (b) WNP, (d) EM3, (f) EM6 (mass load on the suspension system $m = 50$ kg).

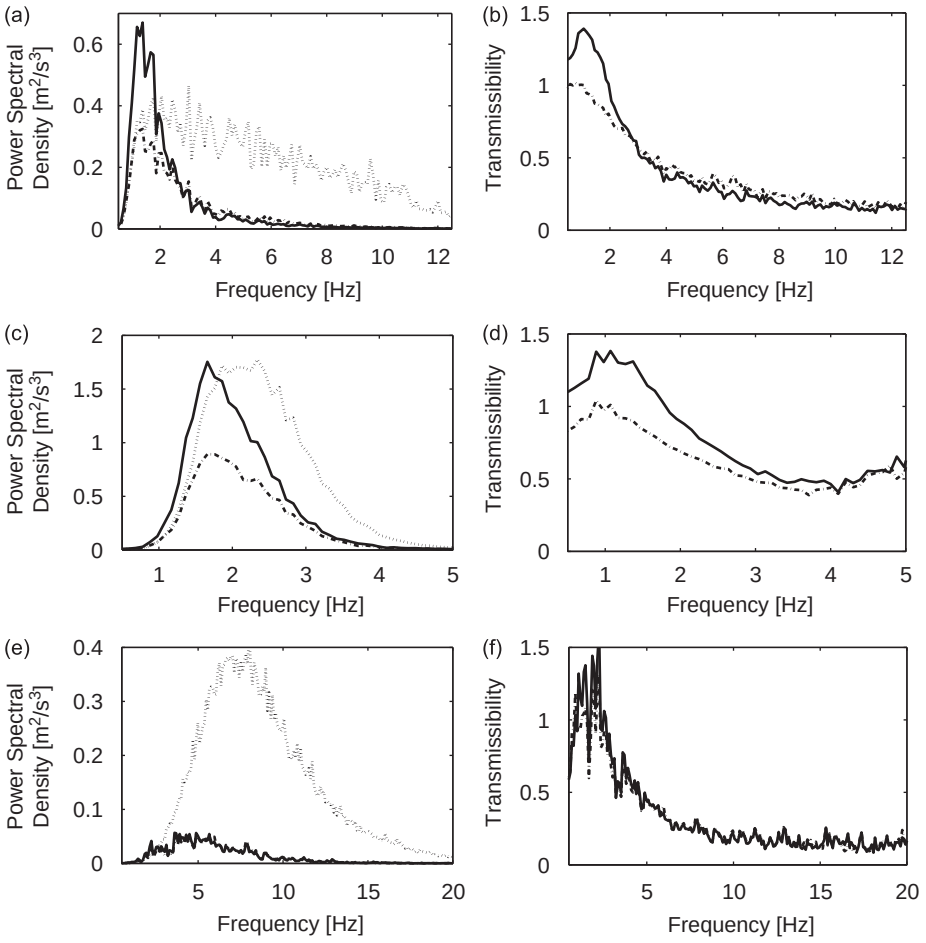

Fig. 16. Measured power spectral densities of conventional (——) and modified (-·-·-) seat suspensions for excitation (·····) signals: (a) WNP, (c) EM3, (e) EM6 and transmissibility curves of seat suspensions for excitation signals: (b) WNP, (d) EM3, (f) EM6 (mass load on the suspension system $m = 120\,\text{kg}$).

The measurement results confirm that the vibro-isolating properties of the modified suspension system improved up to a frequency of about 4 Hz. The main improvement was observed for the higher load masses. The vibration transmission at resonance was reduced efficiently and the proposed modification of the suspension system affects the resonance amplitudes significantly. This effect for the low frequency range of excitation signals, i.e. WNP and EM3 is shown.

6. Conclusions

As shown by the results obtained in the paper, the modified seat suspension significantly improves the vibro-isolating properties of the seat in the 0–4 Hz frequency range. For a higher frequencies, vibro-isolating properties of both seats (conventional and modified) are nearly the same. The best effect of the modified seat suspension is achieved at the resonance frequency of the corresponding conventional passive seat (about 1.3 Hz). Additionally, the procedure proposed in the paper leads to the best compromise between the required reduction of the vibration transmitted to the machine operator and the opposing requirement for reduction of the seat suspension travel. This strategy of improving the seat suspension vibro-isolation properties contributes to better health protection of the operator while maintaining the controllability of the working machine.

Acknowledgements

This work is supported by the Polish Ministry of Science and Higher Education research grant (Project no. N N501 326135, years: 2008–2010). We thank Isringhausen GMBH and CO. KG for the assistance in the experimental research.

Appendix A. Parameter values used for the seat suspension model

Surface of additional air reservoir (A_{add})	$0.1\,\text{m}^2$
Surface of air-spring (A_{as})	$0.1\,\text{m}^2$
Effective area of air-spring (A_{ef})	$7.164 \times 10^{-3}\,\text{m}^2$
Critical pressure ratio (b)	0.5
Critical conductance (C)	$1.322 \times 10^{-8}\,\text{m}^3/(\text{s Pa})$
Linear damping coefficient (d_1)	$5.96 \times 10^3\,\text{N s/m}$
Quadratic damping coefficient (d_2)	$24.34 \times 10^3\,\text{N (s/m)}^2$
Cubic damping coefficient (d_3)	$237.8 \times 10^3\,\text{N (s/m)}^3$
Lower limit of suspension travel without contact with bottom buffers (d_d)	0.061 m
Upper limit of suspension travel without contact with top buffers (d_u)	0.207 m
Gravity constant (g)	$9.81\,\text{m/s}^2$
Initial height of air-spring (h_0)	0.042 m
Linear stiffness coefficient (bottom buffers) (k_{d1})	$6.38 \times 10^3\,\text{N/m}$
Cubic stiffness coefficient (bottom buffers) (k_{d3})	$818 \times 10^6\,\text{N/m}^3$
Stiffness of a seat suspension at the change of movement direction (k_{ff})	$215 \times 10^3\,\text{N/m}$
Linear stiffness coefficient (top buffers) (k_{u1})	$63.9 \times 10^3\,\text{N/m}$
Cubic stiffness coefficient (top buffers) (k_{u3})	$583 \times 10^6\,\text{N/m}^3$
Suspended mass (m)	100 kg
Mass of suspension system affixed to suspended mass (m_s)	7 kg
Atmospheric pressure (p_0)	$1 \times 10^5\,\text{Pa}$
Gas constant (R)	$287\,\text{J/(kg K)}$
Temperature of standard conditions (T_{norm})	293 K
Wall temperature of an air-spring and additional air reservoir (T_w)	293 K
Volume of additional air reservoir (V_{add})	$1.322 \times 10^{-3}\,\text{m}^3$
Overall heat transfer coefficient of an additional air reservoir (α_{add})	$25\,\text{W/(m}^2\,\text{K)}$
Overall heat transfer coefficient of an air-spring (α_{as})	$25\,\text{W/(m}^2\,\text{K)}$
First parameter regulating the shape of a hysteresis model (β)	$2 \times 10^3\,\text{m}^{-1}$
Second parameter regulating the shape of a hysteresis model (γ)	$2 \times 10^3\,\text{m}^{-1}$
Reduction ratio of an air-spring (δ_{as})	2.88
Reduction ratio of a shock-absorber (δ_d)	3.1286
Adiabatic coefficient (κ)	1.4
Density of standard conditions (ρ_{norm})	$1.293\,\text{kg/m}^3$

References

[1] International Organization for Standardization, ISO 7096. *Earth-moving machinery—Laboratory Evaluation of Operator Seat Vibration*, Geneva, 2000.

[2] Z. Engel, *Environment Protection Against Vibration and Noise*, PWN, Warsaw, 1993 (in Polish).

[3] International Organization for Standardization, ISO 2631-2. *Mechanical vibration and shock—evolution of human exposure to whole-body vibration*, Geneva, 1997.

[4] M.J. Griffin, *Handbook of Human Vibration*, London, 1996.
[5] I. Hostens, H. Ramon, Descriptive analysis of combine cabin vibrations and their effect on the human body, *Journal of Sound and Vibration* 266 (2003) 453–464.
[6] M. Nader, *Modeling and Simulation of Influence of Vibrations of Vehicles on Human Body*, Technical University of Warsaw Press, Warsaw, 2001 (in Polish).
[7] J. Kowal, *Vibration Control*, Krakow, Gutenberg, 1996 (in Polish).
[8] T.P. Gunston, J. Rebelle, M.J. Griffin, A comparison of two methods of simulating seat suspension dynamic performance, *Journal of Sound and Vibration* 278 (2004) 117–134.
[9] I. Hostens, K. Deprez, H. Ramon, An improved design of air suspension for seats of mobile agricultural machines, *Journal of Sound and Vibration* 276 (2004) 141–156.
[10] P. Kennes, J. Anthonis, L. Clijmans, H. Ramon, Construction of a portable test rig to perform experimental modal analysis on mobile agricultural machinery, *Journal of Sound and Vibration* 228 (2) (1999) 421–441.
[11] T. Krzyzynski, I. Maciejewski, S. Chamera, Modelling and simulation of active system of truck seat vibroisolation with biomechanical model of human body under real excitations, VDI Berichte No. 1821, 2004, pp. 377–390.
[12] T. Krzyzynski, I. Maciejewski, S. Chamera, On application of fuzzy logic in active control of track driver's seat, *Machine Dynamics Problems* 28 (1) (2004) 91–100.
[13] C.-M. Lee, A.H. Bogatchenkov, V.N. Goverdovskiy, Y.V. Shynkarenko, A.I. Temnikov, Position control of seat suspension with minimum stiffness, *Journal of Sound and Vibration* 292 (2006) 435–442.
[14] J.L. Niekerka, W.J. Pielemeierb, J.A. Greenberg, The use of seat effective amplitude transmissibility (SEAT) values to predict dynamic seat comfort, *Journal of Sound and Vibration* 260 (2003) 867–888.
[15] G. Stein, New results on an electropneumatic active seat suspension system, *Proceedings of the Institution of Mechanical Engineers, Part D*: *Journal of Automobile Engineering*, vol. 214 (5), 2000, pp. 533–544.
[16] G. Stein, Hybrid control system for an AVC unit, *Archives of Control Sciences* 13 (XLIX) (2003) 157–175.
[17] G.J. Stein, P. Mucka, Modelling of the vertical vibration isolating system of the truck test seat, Competitive and Sustainable Growth (GROWTH) Programme, 2004.
[18] K. Toyofuku, Ch. Yamada, T. Kagawa, T. Fujita, Study on dynamic characteristic analysis of air spring with auxiliary chamber, *JSAE Review* 20 (1999) 349–355.
[19] R. Alkhatiba, G. Nakhaie Jazarb, M.F. Golnaraghi, Optimal design of passive linear suspension using genetic algorithm, *Journal of Sound and Vibration* 275 (2004) 665–691.
[20] E. Haller, Device and method for suspension of a vehicle seat by means of additional volumes, United States Patent 20060278805, 2005.
[21] A. Preumont, *Vibration Control of Active Structures—An Introduction*, Kluwer Academic Publishers, London, 2002.
[22] P. Beater, *Pneumatic Drives, System Design, Modelling and Control*, Springer, Berlin, Heidelberg, 2007.
[23] E.W. Gerc, *Pneumatic Drives*, *Theory and Calculation*, WNT, Warsaw, 1973 (in Polish).
[24] W. Tarnowski, *Simulation and Optimisation in Matlab*, Intergraf S.C., Sopot, 2001 (in Polish).
[25] International Organization for Standardization, ISO 6358. *Pneumatic fluid power—components using compressible fluids—determination of flow-rate characteristics*, Geneva, 1989.